CARBON letters

Original Articles
Carbon Letters Vol. 14, No. 3, 175-179 (2013)

Micro-Raman characterization of isolated single wall carbon nanotubes synthesized using Xylene

Young Chul Choi*

Carbon Nanotube Team, Hanwha Chemical Corporation, Incheon 403-030, Korea

Article Info

Received 1 June 2013
Accepted 12 July 2013

***Corresponding Author**
E-mail: youngchoi@hanwha.com
Tel: +82-32-513-7114

Open Access

DOI: http://dx.doi.org/10.5714/CL.2013.14.3.175

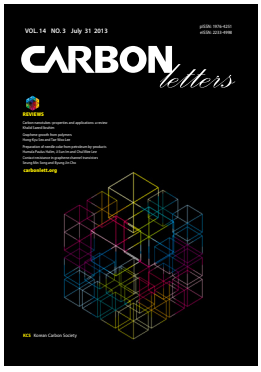

http://carbonlett.org

pISSN: 1976-4251
eISSN: 2233-4998

Abstract

Isolated single wall carbon nanotubes (SWCNTs) were synthesized by chemical vapor deposition (CVD) using a liquid precursor (xylene) as a carbon source. Transmission electron microscopy (TEM) and atomic force microscopy confirmed the isolated structure of the SWCNTs. Micro-Raman measurements showed a tangential G-band peak (1590 cm^{-1}) and radial breathing mode (RBM) peaks (150-240 cm^{-1}). The tube diameters determined from the RBM frequencies are in good agreement with those obtained from TEM. The chirality of the isolated SWCNTs could be determined based on the energy of the laser and their diameter. A further preliminary study on the nitrogen doping of isolated SWCNTs was carried out by the simple use of acetonitrile dissolved in the precusor.

Key words: isolated single wall carbon nanotubes, liquid precusor, Raman spectroscopy, doping

1. Introduction

Single wall carbon nanotubes (SWCNTs) continue to attract extensive interest because of their unique electronic, structural, and mechnical properties [1,2]. These unique and superb properties make SWCNTs good candidates for application in various fields, such as nano-electronics [3], information displays [4], energy storage mediums [5], atomic force microscopy (AFM) [6], and so on. These application fields prefer isolated SWCNTs to bundled ones since the isolated SWCNT has several advantages over its counterpart. For instance, the narrow diameter of an isolated SWCNT is very useful as a field emission tip and AFM probe. Its large specific surface area is extremely important in vehicle energy storage, and sensor applications. In particular, isolated SWCNTs are specifically requested for SWCNT-based nano-electronics because bundled SWCNTs contain both semiconducting and metallic nanotubes, which alters their properties and function.

To utilize SWCNTs in these applications, many researchers have tried to synthesize isolated nanotubes using various techniques, such as arc-discharge [7], laser vaporization [8], and chemical vapor deposition (CVD) [9]. However, due to the very strong van der Waals force between individual nanotubes, most SWCNTs produced so far are in a bundled state, which are not useful for practical applications. For this reason, there have been a number of studies on the nano-dispersion (de-bundling) of SWCNTs as a second-best alternative to producing them singly [10-12].

Among the application fields mentioned above, one of the most intriguing applications is the use of carbon nanotubes in nano-electronic devices, since the feature size of current electronic devices has already reached the minimum state for practical fabrication. Producing a nanosized device using isolated SWCNTs is expected to open the next generation of the semiconducting electronics industry. Such nano-electronics would require isolated SWCNTs doped with n-type or p-type dopants. The synthesis of isolated SWCNTs has been reported on oxidized silicon [13] and AFM probe [14] by CVD using ethylene gas as a carbon source.

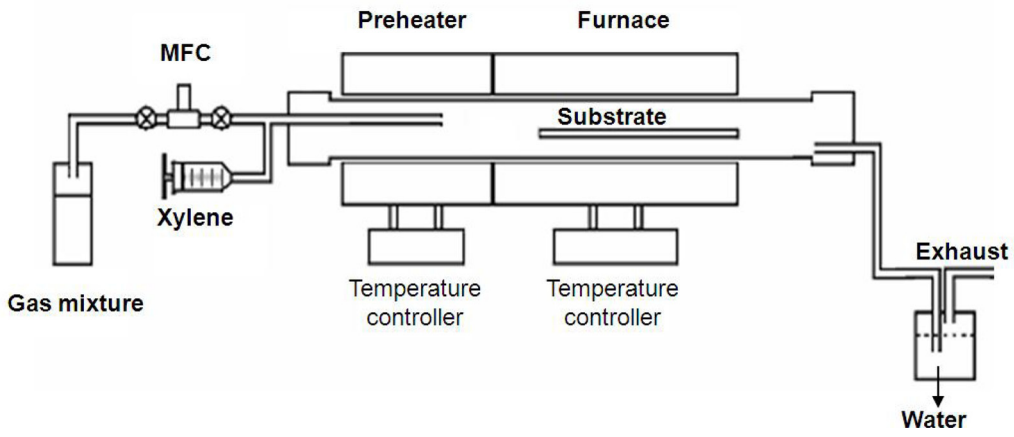

Fig. 1. Schematic diagram of chemical vapor deposition apparatus.

However, it is not straightforward to dope SWCNTs when they are produced by hydrocarbon gas sources, such as ethylene.

In the present study, we synthesized isolated SWCNTs on quartz and silicon oxide substrates by the CVD method using liquid state xylene as a carbon source. This liquid precusor-based growth makes it possible to produce doped isolated SWCNTs by adding soluble dopants into the precursor. A preliminary study on the synthesis of nitrogen-doped isolated SWCNTs was also carried out to demonstrate the potential of this doping method.

2. Experimental

Isolated SWCNTs were grown on quartz and thermally oxidized silicon substrates by CVD using xylene as a carbon source. Iron (III) nitrate nonahydrate powder was dissolved in 2-propanol. The substrates were dipped in this solution for 10 s and then immersed in hexane for 1 s. The substrates were loaded in a quartz tube reactor (1.5" in dia.) and then heated to 750°C with a heating rate of 24°C/min. While the temperature was being increased, argon and hydrogen gases were flowed with flow rates of 600 sccm and 400 sccm, respectively. As soon as the temperature was stabilized at 750°C, xylene was injected into the quartz reactor for 30 min, then the furnace was cooled down under argon atmosphere. Fig. 1 shows the schematic diagram of the CVD used in this study. We used a two-step CVD that is composed of low and high temperature zones. Xylene is injected into the low temperature zone where the temperature is 200°C. Injected xylene is vaporized in this zone, and then carried to the high temperature zone (750°C) by the argon and hydrogen gases.

To investigate the morphologies of the carbon nanotubes grown on the substrates, they were scanned by AFM. Transmission electron microscopy (TEM) was used to measure the diameters of the SWCNTs and to confirm they were isolated single-walled structures. For TEM measurements, we grew SWCNTs directly on silicon oxide-coated TEM grids using the same process of isolated SWCNT growth. A Raman microscope with a focusing area of 1 μm in diameter was also used to analyze the SWCNTs. The excitation wavelength of the laser was 785 nm, corresponding to E_{laser} = 1.58 eV. Based on the Raman spectra, we could determine diameters, chiralities, and the metallic/semiconducting nature of isolated SWCNTs.

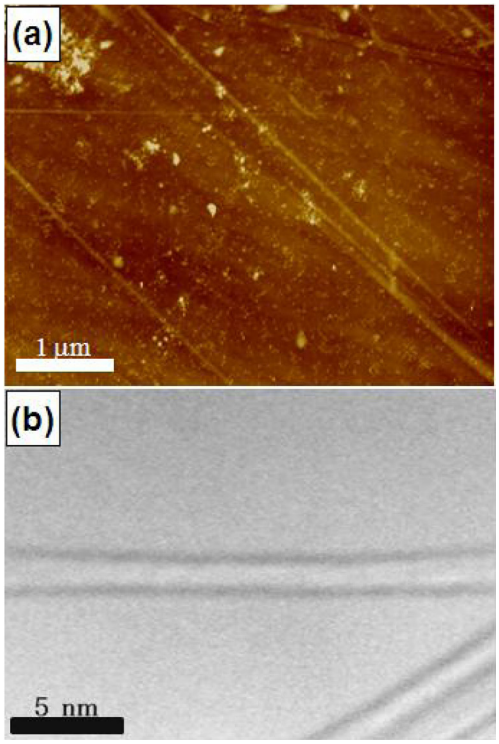

Fig. 2. (a) Atomic force microscopy image of isolated single wall carbon nanotubes (SWCNTs) grown on quartz substrate. (b) Transmission electron microscopy (TEM) image of isolated SWCNTs grown directly on silicon oxide-coated TEM grid.

3. Results and Discussion

Fig. 2a is an AFM image showing isolated SWCNTs synthesized on a quartz substrate. It can clearly be seen that isolated SWCNTs have been successfully synthesized by this process. The SWCNTs have a very straight morphology, indicating high crystallinity. The height profile observed during AFM measurement revealed that the diameters of the isolated SWCNTs ranged

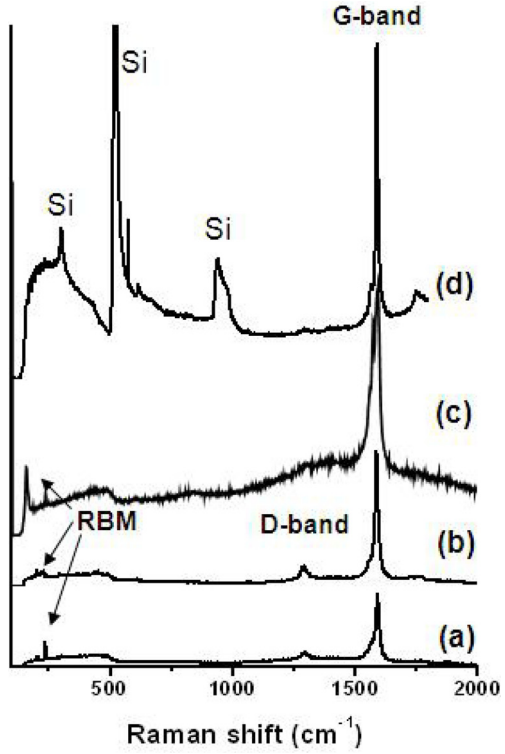

Fig. 3. Raman spectra of isolated single wall carbon nanotubes grown on quartz (a-c) and oxidized silicon (d) substrates. RBM: radial breathing mode.

from 1 nm to 2 nm. Fig. 2b shows a TEM image confirming the isolated single-walled structure of the synthesized nanotubes. The diameters observed in the TEM image ranged from 1.2 to 1.7 nm, which is in good agreement with the AFM observations. It is believed that the variation of nanotube diameter originates from the different sizes of catalyst particles. In order to grow the isolated SWCNTs seen in Fig. 2a, 3 mg of iron (III) nitrate nonahydrate powder was dissolved in 20 mL of 2-propanol so as to form catalytic iron particles on the substrate. It was found that the density of isolated SWCNTs could be controlled by varying the concentration of iron (III) nitrate nonahydrate/2-propanol solution. We observed a noticeable decrease in the number of SWCNTs when the amount of 2-propanol was increased to 40 ml. The isolated SWCNTs could also be synthesized on thermally oxidized silicon substrate, as verified in the following Raman spectra (Fig. 3). However, we could not achieve the growth of SWCNTs on bare silicon substrate. We speculate that the polished surface of the bare silicon substrate is too smooth to nucleate SWCNTs.

The Raman spectra of isolated SWCNTs grown on quartz and thermally oxidized silicon substrates are presented in Fig. 3. The spectra were taken with a focusing diameter of 1 μm using a laser with excitation wavelength of 785 nm, corresponding to 1.58 eV. Figs. 3a-c are the Raman spectra obtained at three different positions on the quartz substrate, and Fig. 3d shows the spectrum of SWCNTs synthesized on thermally oxidized silicon substrate. Tangential G-band peaks around 1590 cm^{-1} were detected with shoulder peaks in the low wavenumber region in all spectra, indicating good formation of SWCNTs [15]. The intensity of the

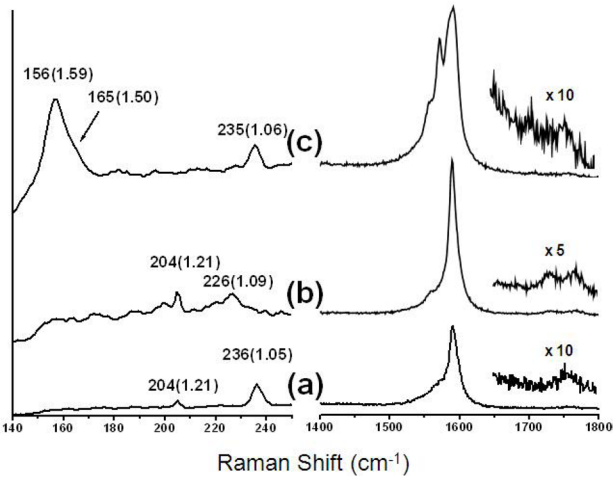

Fig. 4. Raman spectra of isolated single wall carbon nanotubes showing radial breathing modes and G-band peaks of three different positions of a quartz substrate.

disorder induced D-band around 1300 cm^{-1} is small enough to be neglected, meaning that amorphous carbon particles and defects such as pentagons and heptagons in the nanotube structures were hardly formed during the growth process. Radial breathing mode (RBM) peaks are seen in the three spectra obtained from the quartz substrates, although their frequencies are different from each other. The different wavenumbers of the RBM peaks originate from the difference in diameters of the isolated SWCNTs. Although an RBM peak is not seen in the sample grown on the oxidized silicon substrate, shown in Fig. 3d, we believe that there are RBM peaks buried in the broad (100 to 500 cm^{-1}) silicon peak, since the second order Raman peak at around 1750 cm^{-1} in Fig. 3d is due to the combination of RBM and tangential mode [16].

Fig. 4 shows three Raman spectra in the RBM region and the G-band taken from three different regions on a quartz substrate. Each spectrum in the figure has at least two RBM modes, which means that there were at least two isolated SWCNTs in the laser focusing area of 1 μm diameter. This could be expected from the AFM image seen in Fig. 2. The RBM peak frequency, ω_{RBM}, is inversely proportional to the diameter of the SWCNT (d_t) with a relation of ω_{RBM} [cm^{-1}] = 248 cm^{-1}nm/ d_t [nm]. The diameters of the nanotubes calculated from the above relation appear in parentheses. The range of the calculated diameters, from 1.05 nm to 1.59 nm, is in agreement with those obtained from AFM and TEM measurements.

The chirality (n, m) of a nanotube can be determined if a nanotube is within the resonant window, in Kataura's plot [17], of a single available laser excitation line, which is satisfied for E_{laser} within ~ ± 0.1 eV of an interband transition for that nanotube [18]. By applying E_{laser} = 1.58 eV and the estimated diameters into the Kataura plot, it was found that the SWCNTs with diameters of 1.59 nm and 1.50 nm (Fig. 4c) are metallic, and the nanotubes with diameters of 1.05 nm, 1.09 nm, and 1.06 nm in Figs. 4a-c, respectively, are semiconducting. Two nanotubes with diameters of 1.21 nm in Figs. 4a and b are not found in Kataura's plot. Therefore, we could not analyze those nanotubes. Dresselhaus et al. [18] reported the possible chiralities predicted for

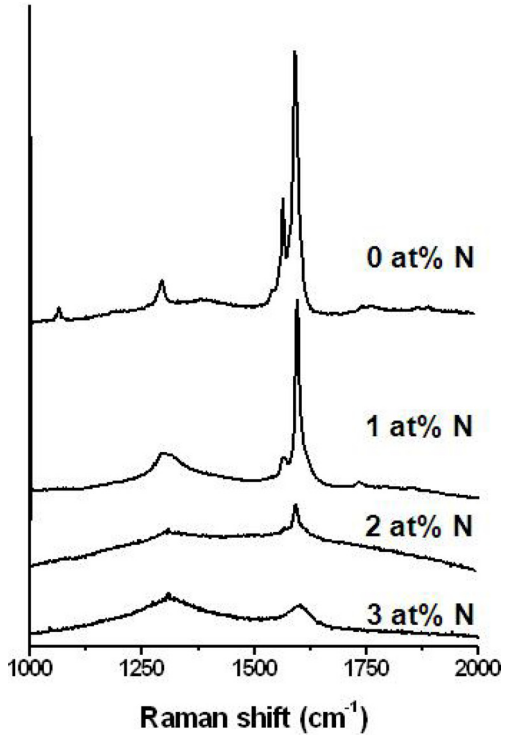

Fig. 5. Variation of Raman spectrum of nitrogen-doped isolated single wall carbon nanotubes with doping concentration.

metallic and semiconducting nanotubes and their calculated ω_{RBM} in the resonant window $1.48 < E_{ii} < 1.58$ eV for $E_{laser} = 1.58$ eV, where $E_{ii} = E_{11}$ for metallic SWCNTs and $E_{ii} = E_{22}$ for semiconducting SWCNTs. With reference to these data, the chiralities of the nanotubes grown in this study could be predicted as follows. The chiralities of the metallic SWCNTs with diameters of 1.59 nm and 1.50 nm in Fig. 4c are (17, 5) or (13,10) and (15, 6), respectively, and the three semiconducting SWCNTs with diameters of 1.06 nm, 1.09 nm, and 1.05 nm might have chiralities of (11, 4), (9, 7), and (10, 5), respectively.

Note that Fig. 4 represents the different morphologies of the tangential G-band peaks located at around 1590 cm^{-1}. The G-band is an intrinsic feature of all sp^2 carbon materials since it is derived from the Raman-allowed optical mode E_{2g} of 2D graphite [19]. The distinctive feature of SWCNTs is that the G-band of a SWCNT has two dominant components, which are ascribed to vibrations along the circumferential direction (lower frequency, ω_G^-) and along the direction of the nanotube axis (higher frequency, ω_G^+). One of the most interesting features of the Raman spectra of SWCNTs is that the G-band shape of a semiconducting SWCNT is different from that of a metallic nanotube. The higher frequency component, ω_G^+, of a semiconducting SWCNT showing a sharp Lorentzian feature [20] with a full width at half maximum of 6-15 cm^{-1}, is similar in shape to that of a metallic one. The lower frequency component, ω_G^-, of a semiconducting SWCNT also has a Lorentzian line shape. However, the ω_G^- of a metallic SWCNT is a very broad Breit-Wigner-Fano (BWF) line [21]. The G-band spectra of Figs. 4a and b show a typical semiconducting feature with ω_G^+ (~1590 cm^{-1}) and ω_G^- (~1560 cm^{-1}). On the other hand, the Raman spectrum of Fig. 4c is different from those of Figs. 4a and b. A broad peak that has been reported as a BWF line is shown in the lower wavenumber region, which indicates that this spectrum results mainly from metallic isolated SWCNTs. This is in agreement with the RBM peaks located at 156 and 165 cm^{-1} which were determined to be from metallic nanotubes.

The advantage of our synthesis technique is that the growth of doped isolated SWCNTs was easily achieved by using liquid precursor (xylene) as the carbon source. Specifically, nitrogen-doped (n-type) SWCNTs could be achieved using acetonitrile that is soluble into xylene. A preliminary study on the synthesis of nitrogen doped SWCNTs was carried out, and its Raman spectra are shown in Fig. 5. The amount of nitrogen to carbon in the precursor ranged from 0 to 3 at%. With increasing nitrogen atomic content, the intensity of the tangential G-band peak decreased, and finally, at 3 at%, the G-band peak, a characteristic feature of single walled SWCNTs, disappeared. In addition, the ratio of the intensity of G-band to D-band (I_G/I_D) decreased dramatically at a nitrogen content over 2 at%, which implies that the incorporation of nitrogen atoms induces significant disorder in the graphene sheet of the isolated SWCNTs. This is also comfirmed by the appearence of D'-band peaks located at around 1610 cm^{-1} (shoulder peaks at the high wavenumber region of G-band) in the spectra of 1 and 2 at% samples.

4. Conclusions

Isolated SWCNTs were successfully grown on quartz and oxidized silicon substrates using xylene as the carbon source. The diameters of the SWCNTs ranged from 1 to 2 nm, as measured by AFM, TEM, and Raman analyses, and their chiralities were predicted based on the energy of the laser and their diameter. Analyses of the RBM and tangential G-band peaks showed that both metallic and semiconducting SWCNTs were being synthesized on a substrate. Nitrogen-doped isolated SWCNTs were also synthesized by adding acetonitrile to xylene. The crystallinity of the doped SWCNTs was found to decrease as the nitrogen content increased.

References

[1] Jeong MS, Han JH, Choi YC. Influence of the purification process on the semiconducting content of single-walled carbon nanotubes synthesized by arc discharge. Carbon, **57**, 338 (2013). http://dx.doi.org/10.1016/j.carbon.2013.01.081.

[2] Jin FL, Park SJ. Recent advances in carbon-nanotube-based epoxy composites. Carbon Lett, **14**, 1 (2013). http://dx.doi.org/10.5714/CL.2013.14.1.001.

[3] Choi WB, Chae S, Bae E, Lee JW, Cheong BH, Kim JR, Kim JJ. Carbon-nanotube-based nonvolatile memory with oxide-nitride-oxide film and nanoscale channel. Appl Phys Lett, **82**, 275 (2003). http://dx.doi.org/10.1063/1.1536713.

[4] Lee H, Jeon J, Goak J, Kim KB, Lee N, Choi YC, Kim HS, Sun J, Park Y, Park J. Ozone electrical trimming of carbon nanotubes to improve their field-emission lifetime and uniformity. J Korean Phys Soc, **54**, 185 (2009). http://dx.doi.org/10.3938/jkps.54.185.

[5] Lee SM, Lee YH. Hydrogen storage in single-walled car-

bon nanotubes. Appl Phys Lett, **76**, 2877 (2000). http://dx.doi.org/10.1063/1.126503.

[6] Cheung CL, Hafner JH, Odom TW, Kim K, Lieber CM. Growth and fabrication with single-walled carbon nanotube probe microscopy tips. Appl Phys Lett, **76**, 3136 (2000). http://dx.doi.org/10.1063/1.126548.

[7] Jeong MS, Han JH, Choi YC. Influence of the purification process on the semiconducting content of single-walled carbon nanotubes synthesized by arc discharge. Carbon, **57**, 338 (2013). http://dx.doi.org/10.1016/j.carbon.2013.01.081.

[8] Thess A, Lee R, Nikolaev P, Dai H, Petit P, Robert J, Xu C, Lee YH, Kim SG, Rinzler AG, Colbert DT, Scuseria GE, Tomanek D, Fischer JE, Smalley RE. Crystalline ropes of metallic carbon nanotubes. Science, **273**, 483 (1996). http://dx.doi.org/10.1126/science.273.5274.483.

[9] Hongo H, Yudasaka M, Ichihashi T, Nihey F, Iijima S. Chemical vapor deposition of single-wall carbon nanotubes on iron-film-coated sapphire substrates. Chem Phys Lett, **361**, 349 (2002). http://dx.doi.org/10.1016/S0009-2614(02)00963-6.

[10] Biswas C, Kim KK, Geng HZ, Park HK, Lim SC, Chae SJ, Kim SM, Lee YH, Nayhouse M, Yun M. Strategy for high concentration nanodispersion of single-walled carbon nanotubes with diameter selectivity. J Phys Chem C, **113**, 10044 (2009). http://dx.doi.org/10.1021/jp9017629.

[11] Utsumi S, Kanamaru M, Honda H, Kanoh H, Tanaka H, Ohkubo T, Sakai H, Abe M, Kaneko K. RBM band shift-evidenced dispersion mechanism of single-wall carbon nanotube bundles with NaDDBS. J Colloid Interface Sci, **308**, 276 (2007). http://dx.doi.org/10.1016/j.jcis.2006.12.041.

[12] Ganter MJ, Landi BJ, Worman JJ, Schauerman CM, Cress CD, Raffaelle RP. Variation of single wall carbon nanotube dispersion properties with alkyl amide and halogenated aromatic solvents. Mater Chem Phys, **116**, 235 (2009). http://dx.doi.org/10.1016/j.matchemphys.2009.03.020.

[13] Hafner JH, Cheung CL, Oosterkamp TH, Lieber CM. High-yield assembly of individual single-walled carbon nanotube tips for scanning probe microscopies. J Phys Chem B, **105**, 743 (2001). http://dx.doi.org/10.1021/jp003948o.

[14] Hafner JH, Cheung CL, Lieber CM. Direct growth of single-walled carbon nanotube scanning probe microscopy tips. J Am Chem Soc, **121**, 9750 (1999). http://dx.doi.org/10.1021/ja992761b.

[15] Rao AM, Richter E, Bandow S, Chase B, Eklund PC, Williams KA, Fang S, Subbaswamy KR, Menon M, Thess A, Smalley RE, Dresselhaus G, Dresselhaus MS. Diameter-selective Raman scattering from vibrational modes in carbon nanotubes. Science, **275**, 187 (1997). http://dx.doi.org/10.1126/science.275.5297.187.

[16] Pimenta MA, Marucci A, Empedocles SA, Bawendi MG, Hanlon EB, Rao AM, Eklund PC, Smalley RE, Dresselhaus G, Dresselhaus MS. Raman modes of metallic carbon nanotubes. Phys Rev B, **58**, R16016 (1998). http://dx.doi.org/10.1103/PhysRevB.58.R16016.

[17] Kataura H, Kumazawa Y, Maniwa Y, Umezu I, Suzuki S, Ohtsuka Y, Achiba Y. Optical properties of single-wall carbon nanotubes. Synth Met, **103**, 2555 (1999). http://dx.doi.org/10.1016/S0379-6779(98)00278-1.

[18] Dresselhaus MS, Dresselhaus G, Jorio A, Souza Filho AG, Saito R. Raman spectroscopy on isolated single wall carbon nanotubes. Carbon, **40**, 2043 (2002). http://dx.doi.org/10.1016/S0008-6223(02)00066-0.

[19] Dresselhaus MS, Eklund PC. Phonons in carbon nanotubes. Adv Phys, 49, 705 (2000). http://dx.doi.org/10.1080/000187300413184.

[20] Jishi RA, Venkataraman L, Dresselhaus MS, Dresselhaus G. Phonon modes in carbon nanotubules. Chem Phys Lett, **209**, 77 (1993). http://dx.doi.org/10.1016/0009-2614(93)87205-H.

[21] Brown SDM, Jorio A, Corio P, Dresselhaus MS, Dresselhaus G, Saito R, Kneipp K. Origin of the Breit-Wigner-Fano lineshape of the tangential G-band feature of metallic carbon nanotubes. Phys Rev B, **63**, 155414 (2001). http://dx.doi.org/10.1103/PhysRevB.63.155414.